New Journal of Physics
The open-access journal for physics

Bouncing trimer: a random self-propelled particle, chaos and periodical motions

S Dorbolo, F Ludewig and N Vandewalle
GRASP, Physics Department B5, University of Liège, B-4000 Liège, Belgium
E-mail: s.dorbolo@ulg.ac.be

New Journal of Physics **11** (2009) 033016 (22pp)
Received 21 August 2008
Published 12 March 2009
Online at http://www.njp.org/
doi:10.1088/1367-2630/11/3/033016

Abstract. A trimer is an object composed of three centimetrical stainless steel beads equidistant from each other and is predestined to show richer behaviour than a bouncing ball or a bouncing dimer. A rigid trimer was placed on the plate of an electromagnetic shaker and was vertically vibrated according to a sinusoidal signal. The horizontal translational and rotational motions of the trimer were recorded for a range of frequencies between 25 and 100 Hz, while the amplitude of the forcing vibration was tuned to obtain maximal acceleration of the plate up to 10 times gravity. Several modes have been detected such as, e.g., rotational and pure translational motions. These modes are found at determined accelerations of the plate and do not depend on the frequency. Chaotic behaviour is observed for other accelerations. By recording the time delays between two successive contacts when the frequency and the amplitude are fixed, a map of the bouncing regime was constructed and compared with that of the dimer and the bouncing ball. Period-2 and period-3 orbits were experimentally observed. In these modes, according to observations, the contact between the trimer and the plate is persistent between two successive jumps. This persistence erases the memory of the jump preceding the contact. A model based on the conditions for obtaining persistent contact is proposed and allows us to explain the values of the particular accelerations for which period-2 and period-3 modes were observed. Finally, numerical simulations allow us to reproduce the experimental results. This allows us to conclude that the friction between the beads and the plate is the major dissipative process.

Contents

1. Introduction

The bouncing ball is a well-known problem and is more often than not presented as an example for explaining the period doubling route to chaos [1]–[7]. Indeed, the bouncing ball problem enlightens us about how a very basic equation of motion is able to generate chaotic motion. The bouncing ball is also relevant in more complex systems when one of the walls is moving in order to inject some energy into the system. The motion of a ball in a box has been addressed in one dimension, known as the Fermi acceleration problem [1], and in two dimensions through the billiard dynamics with moving walls [8]–[10].

Recently, interest in this subject has been renewed through granular shaken systems [11, 12]. When a large assembly of grains is shaken, compaction, convection or even gas-like behaviours may be observed according to the number of grains and to the acceleration of the plate that vibrates the packing. The packing may be considered as an inelastic bouncing ball [11]. Most of the works were concerned with the description of the bouncing ball or the description of a large number of bouncing balls. However, the shape of the bouncing particles has rarely been considered. Actually, the number of possibilities is huge and parameters are numerous. The difficulty is in fixing the relevant parameters. In the present paper, we have experimentally studied the behaviour of a particular object: a trimer. This object is made of three beads equidistant from each other and linked by rigid rods. This particular shape is relevant to the understanding of the bouncing of complex objects.

1.1. Background

The contact of a single ball with a plate may be modelled by one single point of contact despite the complexity of the microscopic bumps present at the surface of both objects in contact. This simple approach is, however, very fruitful when the bouncing dynamics of the ball is considered. The shock between the bead and the plate is characterized by a single parameter: the coefficient of restitution ε that is given by the ratio between the speed of the ball just before v_{before} and just

after v_{after} the collision. This coefficient eventually depends on the impact speed [13, 14]. When the ball is dropped over the plate, it bounces according to the following relation:

$$v_{\text{after}} = -\varepsilon v_{\text{before}} \tag{1}$$

until inelastic collapse occurs [15]. On the other hand, when a spherical bead is dropped or excited on a horizontal plate that is vertically shaken according to a sinusoid with an amplitude A and a frequency f, the relation becomes

$$v_{\text{after}} = v_{\text{plate}} + \varepsilon(v_{\text{plate}} - v_{\text{before}}), \tag{2}$$

where v_{plate} is the vertical speed of the plate at the moment of impact. The second term describes how the relative impact speed influences the rebound. It can be erased when the restitution is zero, i.e. the ball is totally inelastic or when the relative speed between the plate and the ball is zero. When $\varepsilon \neq 0$, it is possible to obtain stable bouncing modes when the speed provided by the plate during the impact compensates for the energy loss. The relevant parameter is the reduced maximum acceleration Γ defined by the ratio between the maximum acceleration of the plate $A\omega^2$ (ω being the impulsion $2\pi f$, f is the forcing frequency) and gravity g.

The shape of an object is rarely as simple as an ideal sphere. As a consequence, the object is subject to rotation and the coefficient of restitution depends on the orientation of the object and both its translational and rotational speeds. As a first step towards a more complex system than a ball, we may think of the ellipsoid. This object always has one contact with the plate but the 'surface' of the contact depends on the orientation of the object. Moreover, a new degree of freedom is introduced since rotation is allowed. However, it is pretty difficult to experimentally study the dynamics of such a well-defined shape.

On the other hand, an increase in complexity may be obtained by increasing the number of contacts between the object and the plate. The first step, called a dimer, is an object that has two contact points when it is at its stable position on a plate; a dimer is an object formed by two beads linked by a rigid rod. The bouncing of that object on a vertically shaken plate was studied in 2004 [16, 17]. The preliminary investigations concerned the bouncing mode when Γ is below 1 [16]. In these conditions, the bouncing is obtained only when the dimer is excited by dropping it on the plate. Different orbits have been observed. Let us describe them in order of increasing energy:

- The mode G (for ground): the dimer does not bounce and both beads remain in contact with the plate.
- The mode D (for drift): one of the beads bounces, while the other follows the motion of the plate (the latter remains roughly in contact with the plate). The dimer then moves horizontally. Its speed depends on the aspect ratio α_r of the dimer, i.e. the ratio between its length and the bead diameter. Namely, the speed decreases with α_r. Compared with the bouncing ball, this mode is totally new, since it comes from an additional degree of freedom of the dimer, i.e. rotation.
- The mode J (for jump): both beads bounce together and hit the plate once per period. The succession of bounces of beads 1 and 2 follows a complex but periodic sequence.
- The mode T (for twist): each bead alternately hits the plate once every two periods.

A second paper [17] investigates what happens at Γ above one. Transitions between modes have been observed. An interesting description of the bouncing dimer for plate accelerations above g has been developed by Swift *et al* [18]. They showed that a bouncing dimer experiences

stochastic motion regarding the time delay between successive shocks and the angle at the impact moment.

The mode D is very interesting because it represents a way to generate self-propelled particles without introducing a textured substrate as in [19]–[21]. This is particularly useful to study collective behaviours as nicely performed by Kudrolli *et al* [22]. In this work, spontaneous swirling and clustering are observed. The analogy between the self-organization of these grains and biological systems is remarkable.

In that framework, we are interested in generating self-propelled particles. Naturally, a trimer composed of three beads equidistant from each other is a good candidate. Indeed, the co-planar configuration of three beads offers the advantage of being much less sensitive to a slight slope of the plate compared with the dimer. Moreover, we may *a priori* imagine that the horizontal motion of the trimer centre of mass can be erratic. The self-propelled trimer could then be considered as a self-propelled random walker.

1.2. Aims and scope

The aims of the present work are (i) to determine the forcing oscillation conditions for which the trimer behaves as an erratic self-propelled particle and (ii) to compare the bifurcation diagram of a bouncing ball, a bouncing dimer and a bouncing trimer.

By way of an introduction, the video file intro.mov, available from stacks.iop.org/NJP/11/033016/mmedia, shows two situations that illustrate both the aims of the present work. Indeed, on the left, a small trimer (see legend) experiences a random motion on the plate. On the other hand, in the movie on the right, a large trimer bounces randomly before locking into a periodic motion (it bounces once every two periods).

In a first step, the inclination of the trimer will be neglected compared with the horizontal motion of the centre of mass and the rotations around the vertical axis. From this simplified point of view, the motion of the trimer can then be decomposed into the rotation and translation motions. In a second step, the vertical motion will be considered. The latter is rather difficult to obtain by image analysis. That is why we prefer to study the time delay between successive impacts to determine some dynamics of the vertical motion of the beads.

The experimental set-up is detailed in the following section. Subsequently, the paper is split into a section concerning the experimental results (section 3) and a section about the numerical investigations (section 4). Section 3.1 is devoted to the centre of mass motion and to the rotation of the trimer neglecting the vertical motions. On the other hand, section 3.2 is focused on the description of the bouncing mode and the comparison with the bouncing ball and dimer. Numerical investigations have been performed in order to evidence the relevant parameters governing the stable trajectories and chaotic regimes (section 4). Finally, conclusions are drawn.

2. Experimental set-up

The basic beads used in this work are stainless steel beads of 10 mm diameter. They will be considered alone (ball), glued at the extremities of a rigid rod (dimer) or disposed in a triangle (trimer). For dimers, a metallic rod is used and the glue is bi-component epoxy. As for trimers, the centimetrical stainless steel beads are glued on a polycarbonate triangle. The mass of a single bead is 4.1 g. Two trimer sizes have been considered (as justified in the next section). Actually, the trimer is characterized by its aspect ratio α_r given by the ratio between the length of one side and the bead diameter; for example, when three beads are glued to form a triangle, the aspect

ratio of such a trimer is 2. The mass m of the considered trimers are 14.6 and 18.5 g, respectively, to give trimers with $\alpha_r = 3.5$ and 5.6. The mass of the plexiglass supporting plates is then 2.3 and 6.2 g, respectively. The flexion modes of the rod in a dimer and of the triangle in a trimer have not been considered explicitly. However, they are included in the dissipation processes that define the coefficient of restitution of the trimer. This coefficient affects the vertical dissipation processes. On the other hand, the friction of the beads on the plate affects the horizontal motion.

The object under consideration (a bead, a dimer or a trimer) is set on a plate bordered by a squared arena in order to avoid the escape of the object from the plate. The interaction between the borders and the bouncing object may affect the periodical modes. In order to avoid these effects, some authors propose working on a parabolic plate [2, 23]. Such a system can be envisaged for one single bead but does not hold for dimers and trimers. For the dimer, a groove should be better than a parabolic plate. Since no simple solution exists for the trimer, we chose to work on a plane plate (a square of 200 mm sides) and to try to limit the interaction between the bouncing object and the borders. The border–trimer interaction is reduced by gluing a thin disc made of rigid plastic on the top face of the trimer. The radius of this disc is slightly larger than the trimer. By so doing, the trimer and the borders have, at worst, only two contact points. Moreover, this circular shape avoids the trimer being trapped at the corners. The experiment may continue even after a collision with one of the borders. Both circular and square arenas have been compared without any noticeable effect on the results.

The plate is vertically shaken by an electromagnetic shaker (G&W V55) via a linear bearing in order to ensure unidirectional vibration. The considered frequencies are tuned between 20 and 100 Hz, while the amplitude allows us to reach accelerations up to $\Gamma = 10$. The acceleration is measured thanks to a calibrated accelerometer.

The motions of the trimer are recorded using a high-speed camera (IDT Redlake). To begin with, the camera is placed above the plate (results are shown in section 3.2). That allows us to record the horizontal translational and rotational motions of the trimer with respect to the vertical excitation. A high recording speed is not necessary for this purpose (25 images per second is generally enough). On the other hand, to analyse the vertical motion, the camera is placed perpendicular to the axis of vibration and the image acquisition speed is set to 250 images per seconds (results are shown in section 3.3).

Each time that the bouncing object (one bead, a dimer or a trimer) hits the plate, a high and sharp peak is observed in the accelerometer signal. This allows us to measure the time delay Δt between two successive shocks. This method has the disadvantage of not detecting simultaneous shocks and not detecting soft shocks (when the bead and the plate collide with a relative speed close to zero). However, fixing the frequency and the amplitude, a set of time delays Δt can be accumulated. The distribution of these time delays allows us to extract periodical behaviour such as, e.g., phase locking or period doubling.

From the practical point of view, the acceleration of the plate is removed from the accelerometer signal by using a high-pass filter. The signal is then recorded by an oscilloscope and transmitted to a computer. The absolute value of the signal is then cleaned by studying the correlation of the signal and a decreasing exponential $\exp(t/\tau)$, where τ (≈ 1 ms) represents the typical relaxation of the signal after a shock and t is the time. A peak is considered as resulting from a shock when the peak value is larger than a preliminarily determined threshold P that depends on f and A. The function $P(f, A)$ is basically determined by studying the accelerometer signal without any bouncing object on the plate.

To sum up, the measurement procedure is as follows. The frequency is fixed at f. The amplitude range of the plate is chosen in order to sweep reduced accelerations between 0.5 and 10 by a certain amplitude step ΔA. Step one: to begin with, the signal from the accelerometer is recorded and treated when no object is present on the plate. That allows us to determine the threshold values $P(A, f)$. Step 2: after that first run, the shaker is stopped and the object is placed on the plate. Data sets of time delays $\Delta t(A, f)$ are collected for each value of the tuned amplitude. From these sets, the probability distributions of the Δt's are deduced. The density of probability of Δt is mapped on a $(\Delta t, \Gamma)$ plot (the frequency being fixed).

3. Experimental results

3.1. Coefficient of restitution and choice of sizes

For a bead, the characterization of the bouncing is mainly governed by the coefficient of restitution ε. This coefficient is given by the ratio between the speed of the object just before the impact and the speed just after the impact. The coefficient is quite easy to measure for a single bead. For a dimer, things turn out to be more complex since the orientation of the dimer before the impact and the rotations have to be considered. In that case, the friction between the object and the plate must be taken into account since the contacts may be subjected to a torque. However, when the dimer is aligned along the vertical or the horizontal direction and when the dimer does not rotate, the coefficient of restitution is defined as the ratio between the speed after and before the collision with the plate. Finally, it is indeed pretty difficult to define a basic coefficient of restitution for the trimer. Indeed, when the object is too complex, the object tangential speed with the plate may be nonzero. The main consequence is that friction between the bead and the plate must be taken into account. The energy loss processes are the restitution of individual beads, the friction between the beads and the plate and the flexion of the trimer.

As first measurements, the restitution coefficients for one single bead and for a dimer ($\alpha_r = 3.5$) were studied. The dimer was released horizontally and vertically on the plate in order to evidence the range of restitution coefficients. An electromagnet is used to release the dimer on the plate. As the dimer beads are made of magnetic stainless steel, the switch off of the electromagnet allows the dimer to fall without any rotation. A high-speed camera located far enough from the impact site is used to determine the speed of the centre of mass before and after the impact. As the rotation of the dimer is negligible, the horizontality (or verticality) is conserved before and after the impact. In figure 1, the coefficient of restitution is represented. The circles, squares and triangles are for the single bead, the dimer that impacts the plate horizontally and the dimer that impacts the plate vertically, respectively.

The coefficient of restitution of the single bead is found to increase when the impact speed is decreased. Our measurements are consistent with the theoretical behaviour of $\varepsilon(v)$ found in [13] and are scaled by $v^{-1/4}$ (continuous line in figure 1). For the single bead, ε varies between 0.4 when the impact speed is $0.1\,\mathrm{m\,s^{-1}}$ and 0.3 when the speed is larger than $1\,\mathrm{m\,s^{-1}}$. In the following, the coefficient of restitution of a bead impacting a plate will be taken to be equal to 0.35. This value is indeed low compared with the coefficient of restitution of a bead–bead collision.

It is worth noting that the dimer hitting the plate horizontally has the lowest coefficient of restitution of the three considered cases. Indeed, this can be understood by considering the double contacts of the dimer with the plate. At the precise moment of this double event, the two

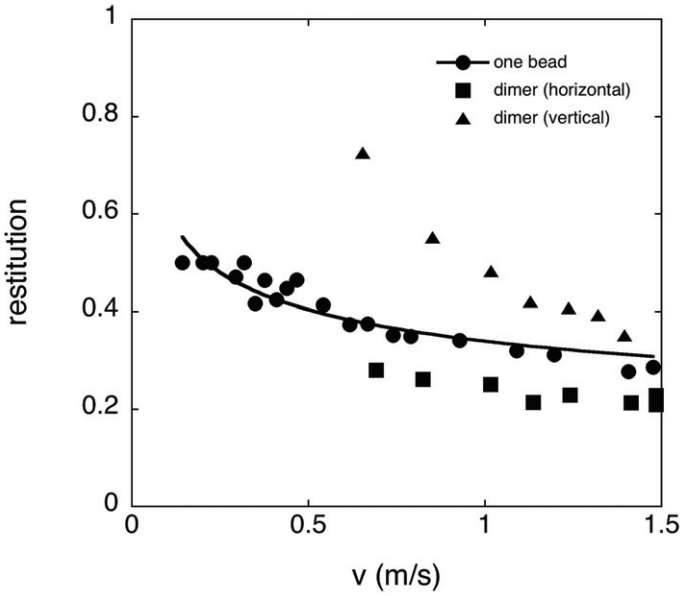

Figure 1. Coefficient of restitution of a bouncing ball (circles), a dimer rebounding vertically (triangles) and a dimer bouncing horizontally (squares) versus the impact speed of the centre of mass.

Table 1. Horizontal drift speed of a dimer. The reduced acceleration is 0.9, and the aspect ratio is indicated.

α_r	Frequency	Speed (cm s^{-1})
3.5	25	2
	50	1
	75	0.7
5.5	From 25 to 75	< 0.1

beads generate a couple of contrary torque on the dimer. The momenta have different signs and this has the consequence of frustrating the dimer; in other words, a lot of energy is dissipated in the elastic deformation of the dimer. On the other hand, when the dimer is vertically released, the coefficient is about twice the coefficient of the horizontal case and thus is larger than the single bead. The large restitution observed with the vertical dimer is attributed to the elasticity of the rod.

As for the choice of the trimer sizes, the experiments realized with bouncing dimers will be relevant. The study of the D-mode reveals to us that the speed (the motility) of such a particle depends on the aspect ratio of the dimer [16]. According to these measurements, the maximal horizontal drift speed of the dimer is found when $\alpha_r = 3.5$. The speed decreases to zero at $\alpha_r = 5.5$. In table 1, the speed of the dimer versus the frequency is given. In order to evidence the aspect ratio role, two trimers have been constructed with aspect ratios equal to 3.5 and 5.6, respectively.

In section 3.2, the horizontal motions (rotation and translation) of the trimer will be studied. The $\alpha_r = 3.5$ trimer will be used. On the other hand, in order to discover the modes and windows of stability, the less mobile $\alpha_r = 5.6$ trimer will be considered in section 3.3.

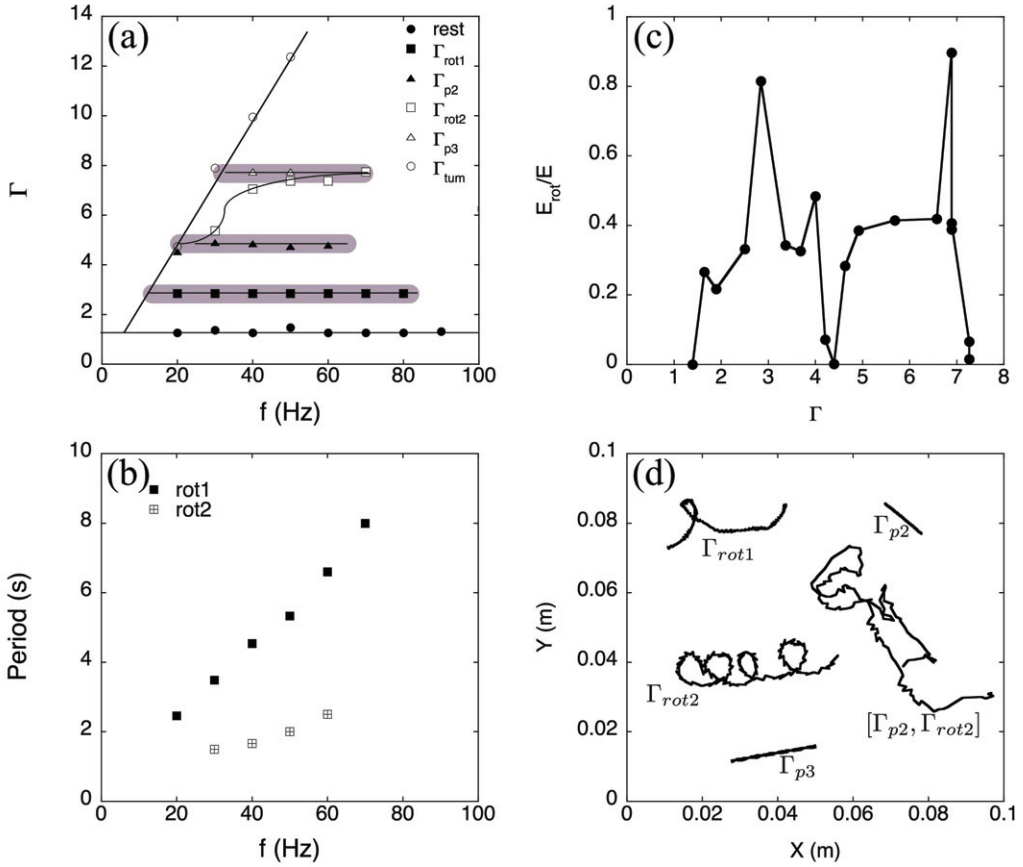

Figure 2. (a) Phase diagram presenting the different modes encountered for a trimer with $\alpha_r = 3.5$ when the frequency f and the reduced acceleration Γ of the vertical excitation are tuned. Below the black bullets, the trimer remains on the plate without bouncing. The trimer locks a periodical orbit along the grey areas that delimit windows of stability. A rotation mode is found when the acceleration value of the plate is located in the grey area with black squares, a period-2 mode in the grey area with black triangles, a second rotation mode along the curve with open squares and a period-3 mode in the grey area with open triangles. The trimer tumbles when excited above the oblique line passing through open circles. (b) Comparison of the rotation period in the mode of rotation 1 (black squares) and in the mode of rotation 2 (open squares) as a function of the forcing frequency. (c) Ratio between the rotational $E_{\rm rot}$ and total energy E of a bouncing trimer at $f = 40$ Hz. (d) Trajectories of the centre of mass of the trimer in the following modes: period-2, rotation-1, rotation-2, period-3 and in a chaos state. The reduced accelerations indicated on the figure refer to the mode. See also the movies intro.mov and sweep.mov, available from stacks.iop.org/NJP/11/033016/mmedia.

3.2. Tracking the trimer motions

To begin with, we vertically shake a trimer with $\alpha_r = 3.5$ because this size corresponds to a very mobile dimer aspect ratio. The diagram of figure 2(a) presents the different encountered modes with respect to the frequency f and the reduced acceleration Γ. The modes occur in stability

windows represented by the grey area in this phase diagram. The symbols are the experimental accelerations for which a particular mode has been observed. To enumerate the different modes, the behaviour of a trimer shaken at 40 Hz will be described hereafter. Starting from $\Gamma = 0$, the trimer remains in contact with the plate until $\Gamma_{\text{rest}} \approx 1.3$. The trimer bounces randomly until $\Gamma_{\text{rot1}} \approx 3$. At that acceleration, it rotates on itself (grey area with black squares), and the horizontal translational energy is zero. Increasing the acceleration slightly conducts the trimer to random translational and rotational motions. When $\Gamma_{\text{p2}} \approx 5$ is reached, the trimer bounces once every two periods. Seen from the top, the horizontal translational and rotational motions are stopped. The plane of the trimer remains parallel to the plate. Increasing the acceleration, random motion is again observed until $\Gamma_{\text{rot2}} \approx 7$. There, a rotation mode is observed, in which rotation speed is larger than the previous rotation mode at $\Gamma = \Gamma_{\text{rot1}}$. Note that this mode is not very stable and is difficult to obtain. At $\Gamma_{\text{p3}} \approx 8$, the trimer bounces once every three periods, and the plane defined by the three beads remains parallel to the plate. Finally, the trimer tumbles for $\Gamma_{\text{tum}} > 10$. The limit accelerations Γ_{rest}, Γ_{rot1}, Γ_{p2}, Γ_{rot2} and Γ_{p3} are represented in figure 2(a). It is remarkable that these particular accelerations do not depend on the frequency. The experiment also shows the stability windows of the bouncing trimer system that depend only on the reduced acceleration Γ. On the other hand, the acceleration for tumbling is observed to vary linearly with the frequency.

A simple argument allows us to explain the latter fact. The trimer may tumble when one of the beads gets enough kinetic energy from the plate to reach a height of at least the length of the bisector of the triangle defined by the beads of the trimer. The maximum accessible speed for a bead can be taken as the maximum speed of the plate $A\omega$. The balance between the kinetic energy and the potential energy can be written as

$$\tfrac{1}{2}m(A_{tum}\omega)^2 = mgh, \tag{3}$$

where h is the length of the bisector and A_{tum} is the plate amplitude for which the trimer tumbles. Inserting the expression of the amplitude with respect to the reduced acceleration, we obtain

$$\Gamma_{\text{tum,th}} = \omega\sqrt{\frac{2h}{g}}, \tag{4}$$

with $\Gamma_{\text{tum,th}}$ being the theoretical reduced acceleration for tumbling. This law shows that the acceleration required for tumbling varies linearly with the frequency.

The movie sweep.mov, available from stacks.iop.org/NJP/11/033016/mmedia shows the dynamics of the trimer when the acceleration is slowly increased from 0 to about $5g$. The rotation and period-2 modes are clearly visible (the frequency was fixed at 25 Hz).

The rotational mode is a kind of generalization of the drift motion observed for the dimer. The propulsion is a consequence of the friction between the beads and the plate [16]. The periods of rotation have been measured for rotation-1 and rotation-2 that occur, respectively, at $\Gamma \approx 3$ and 7. They are presented in figure 2(b) versus the excitation frequency. A period of about 2 s corresponds to a linear speed of a bead of about 3 cm s^{-1}. This is compatible with the measurement of the dimer. The filled and open squares are for mode 1 and mode 2, respectively. The period of rotation increases linearly with the frequency. Indeed, the slowing has also been observed with the dimer, i.e. the linear speed of a dimer scales with the inverse of the frequency as demonstrated in [16].

In order to evaluate the energy E of motion, we do not consider the vertical contribution and the contribution of the polycarbonate triangle; the translational E_{tran} and the rotational E_{rot}

energy have to be calculated:

$$E = E_{\text{tran}} + E_{\text{rot}} = \tfrac{1}{2}Mv^2 + \tfrac{1}{2}I\dot{\phi}^2, \tag{5}$$

where M is the total mass of the trimer, I is the angular momentum and $\dot{\phi}$ is the rotation speed of the trimer. The angular momentum is given by

$$I = 3(md^2 + \tfrac{2}{5}mr^2), \tag{6}$$

where m is the mass of one bead, d is the distance between the centre of mass of the trimer and the centre of mass of one bead and r is the radius of a bead. The energy (horizontal) has been computed thanks to the recording of the trimer trajectories. In figure 2(c), the ratio between the rotational kinetic energy E_{rot} and the total kinetic energy E is plotted with respect to the reduced acceleration Γ, while the frequency is kept constant at 25 Hz. The peaks at $\Gamma = 3$ and 7 correspond to the rotation modes, while the zeros found at $\Gamma = 4.5$ and 7.3 correspond to period-2 and period-3 modes, respectively. It is worth noting that the most chaotic motion is found between $\Gamma = 5$ and 6.5. In that range of forcing acceleration, the rotational energy is nearly equal to the translational energy. Self-propelled random walker particles are thus found in that range of acceleration.

Finally, the trajectories have been recorded during 40 s for five particular accelerations: $\Gamma_{\text{rot1}} < \Gamma_{\text{p2}} < \Gamma_{\text{walk}} < \Gamma_{\text{rot2}} < \Gamma_{\text{p3}}$, where Γ_{walk} is a reduced acceleration of the plate intermediate between Γ_{p2} and Γ_{rot2}. The trajectories are represented in figure 2(d), X and Y being the coordinates of the centre of mass of the trimer on the plate. The period-2 and period-3 modes are characterized by a linear trajectory. The speed is very low ($0.5\,\text{mm}\,\text{s}^{-1}$). This slow drift is the consequence of a small tilt of the plate. On the other hand, the trajectories for both rotational modes are loops. The horizontal speeds are again small ($\approx 1\,\text{mm}\,\text{s}^{-1}$). The trimer, when accelerated at an acceleration between Γ_{p2} and Γ_{rot2}, has a horizontal speed of $5\,\text{mm}\,\text{s}^{-1}$. During the period of time of the measurement (40 s), the trimer randomly turns on itself. This shows that the self-propelled random walker is found in that range of reduced acceleration. However, the recording time is too small to allow us to determine whether the motion is under- or over-diffusive.

3.3. Mapping the trimer bouncing modes

Some modes may not be observed by the eye because they have a long period or are very fast. The time delays between two successive shocks of any beads on the plate have been chosen to map the system with respect to the reduced acceleration while the frequency is fixed. The procedure used to obtain these diagrams is described in section 2. The frequency has been fixed at 25 Hz and since the period is rather large, that allows us to have maximum time resolution. In figure 3, the bouncing ball (top), the bouncing dimer ($\alpha_r = 3.5$) (middle) and the bouncing trimer ($\alpha_r = 5.6$) (bottom) are compared. The darker the plot, the greater the probability of finding the time delay between successive shocks. The experimental method is quite similar to that used in the oscillation of a thin layer of grains [12]. In this section, a large trimer has been used because we know that the horizontal motion is less important than for the small one. In so doing, the interaction with the border is reduced.

Let us begin by describing the bouncing ball diagram. Since only one single ball is considered, the time duration between two successive shocks with the plate also represents the flight time of the bead. This flight time is a well-known parameter and is theoretically related to the logistic map [3]. More often than not, the completely inelastic bouncing ball diagram is

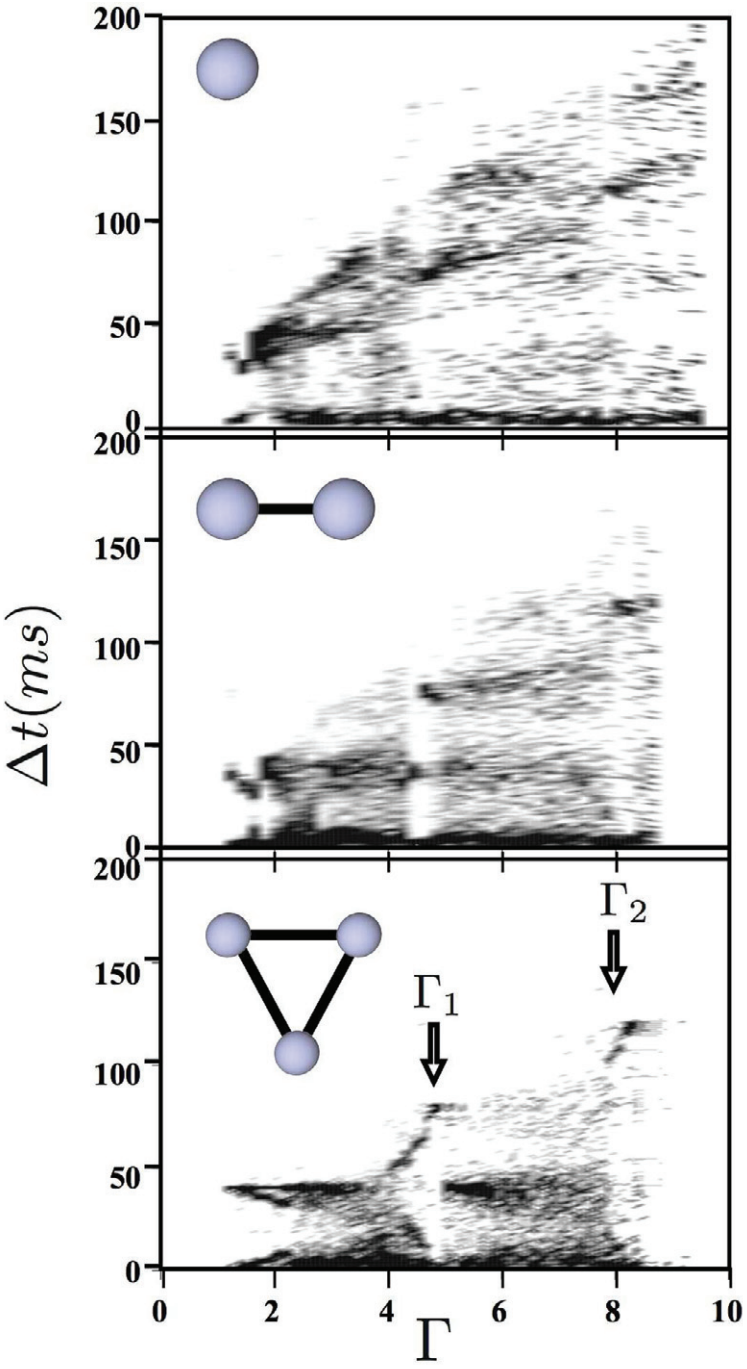

Figure 3. Density of probability of finding a time delay between two successive bead–plate impacts with respect to the reduced acceleration. The darker the plot, the greater the probability of finding the time delay. The frequency is fixed at 25 Hz (period = 40 ms). Three cases are compared: the bouncing ball (top), the dimer ($\alpha_r = 3.5$) and the trimer ($\alpha_r = 5.6$). The arrows indicate the particular values Γ_1 and Γ_2 described by equation (16).

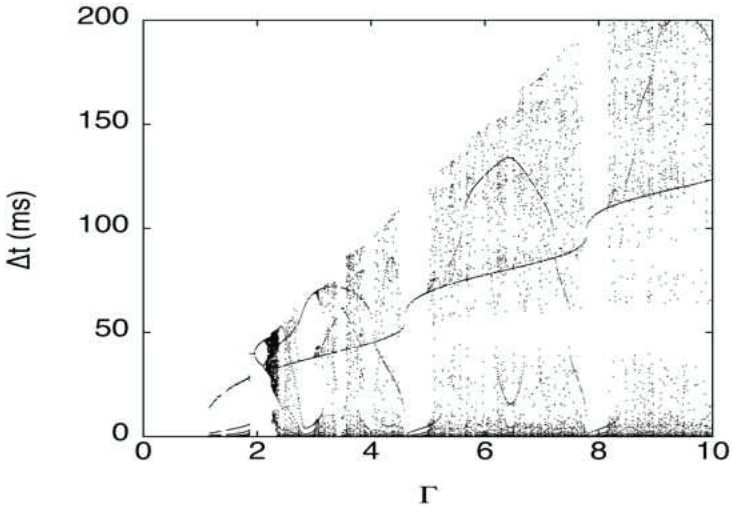

Figure 4. Theoretical map of the time delay between successive impacts for a bouncing ball with a coefficient of restitution of 0.35.

represented because it evidences very clearly the period doubling route to the chaos. In our case, the bouncing is characterized by a certain coefficient of restitution ε, defined as the ratio of the ball speed just before and just after the collision with the plate at rest. This coefficient has been measured with respect to the impact speed. Indeed, we observe an increase of the coefficient when the impact speed goes to zero [13, 14]. The mean value for ε has been found to be 0.35. It is very easy to compute the flight time of the bouncing ball according to the reduced acceleration of the plate when the frequency is fixed. Figure 4 presents the results of the simulation for the bouncing ball with $\varepsilon = 0.35$ and $f = 25$ Hz. The general shape is in good agreement with the experimental bifurcation diagram, especially according to the stability windows and according to the forbidden flight time regions. On the other hand, the period doubling cascade (located between $\Gamma = 2$ and $\Gamma = 3$) cannot be experimentally observed, because the time resolution is not small enough.

When comparing the ball, dimer and trimer diagrams, we observe that generally the time delays between shocks are decreased. This first observation is only natural since the number of beads is increased. Secondly, two stability windows are encountered at $\Gamma \approx 5$ and 8. At these accelerations, period-2 and period-3 orbits are observed for all three of the considered objects. They are characterized by a darker area at ($\Gamma = 5$, $\Delta t = 80$ ms) and ($\Gamma = 8$, $\Delta t = 120$ ms). Note that, at these accelerations, the dimer twists from one bead to the other.

The trimer diagram is the most rich according to the structures that can be observed. No time delay larger than 40 ms is observed for accelerations until $\Gamma = 4$. It is interesting to observe that below $\Gamma = 2$, three branches exist: one is constant at $\Delta t_{\text{branch1}} = 40$ ms and the other two are complementary: $\Delta t_{\text{branch2}} + \Delta t_{\text{branch3}} = 40$ ms. The bouncing order of the three beads is difficult to determine even at $f = 25$ Hz. The dynamics of the contact are pretty delicate to experiment. The motion of the trimer makes an automatic optical detection difficult mainly because the spatial size of the contacts is much lower than the size of the trimer.

Actually, two additional modes have been detected. They occur for accelerations just above Γ_{p2} and Γ_{p3}. The trimer bounces alternately on two of the three beads and then on the third one. This results in a twisting motion of the entire trimer. Moreover, a horizontal and rectilinear

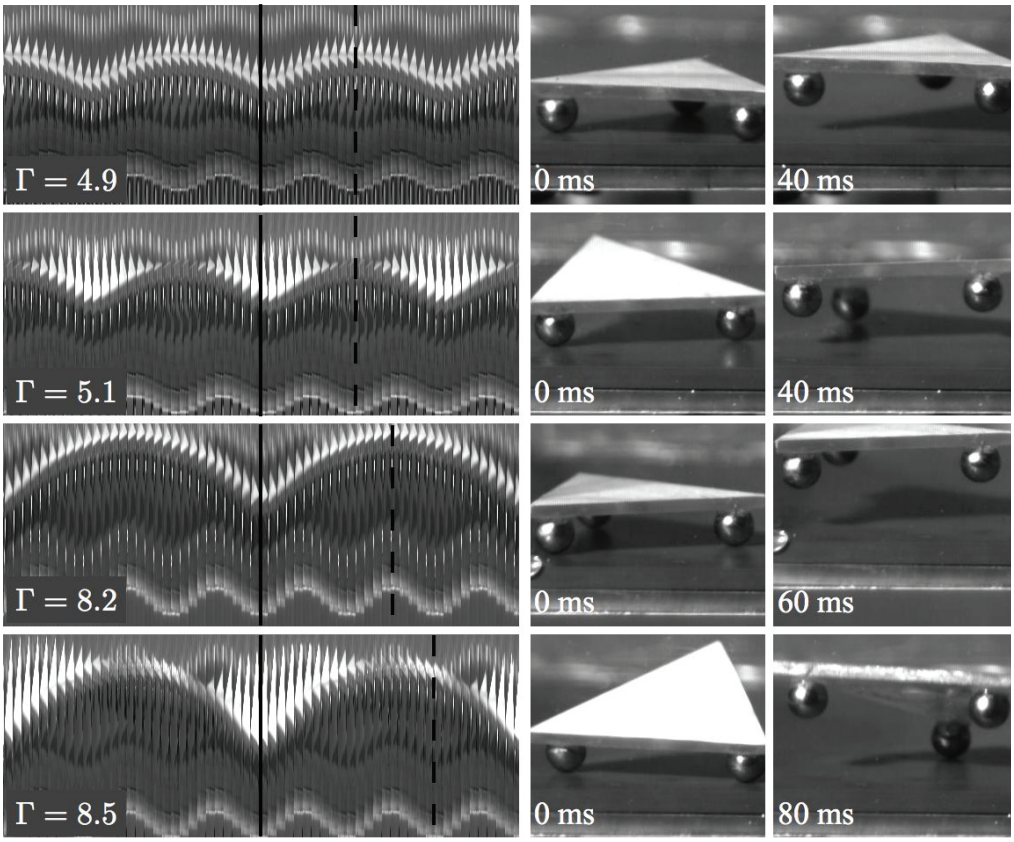

Figure 5. The figure aims to compare the trajectories of the trimer and the plate. From top to bottom, the trimer is in the period-2 mode, in the twist-2 mode, in the period-3 mode and finally in the twist-3 mode. The reduced accelerations are indicated on the left. The two pictures on the right are snapshots of the trimer in the corresponding mode (times are indicated). For each case, a series of 60 snapshots has been juxtaposed, the snapshots having been horizontally shrunk. This allows us to visualize the trajectories of the plate and of the trimer. The sinusoidal curve at the bottom of each picture in the left column represents the motion of the plate, whereas the white sinusoidal-like zone above the plate motion represents the motion of the trimer. The whiter the zone, the more the trimer is inclined. In other words, the white colour indicates the inclination of the trimer. The vertical plain and interrupted lines indicate the times at which the snapshots from the central column and from the right column have been taken. See also the movie diag.mov, available from stacks.iop.org/NJP/11/033016/mmedia, that illustrates the different periodical motions observed.

motion is then observed. The signature of one of these twist modes is seen as a darker area for acceleration just above $\Gamma \approx 5$.

The period-3 orbit is interesting because 'period-3 is a clue for chaotic motion' [24]–[26]. The motion of the centre of mass for reduced accelerations between Γ_{p2} and Γ_{rot2} for the small trimer is certainly chaotic and the random walker characteristic is well checked.

A more precise description of the system is shown in figure 5. Pictures of four particular modes have been taken using the high-speed camera. From top to bottom, the period-2 mode, the twist-2 mode, the period-2 mode and the twist-3 mode are represented (the accelerations are indicated on the left). The two pictures on the right are snapshots taken during the bouncing. The times are indicated in the figures. On the left side of figure 5 are pictures composed by the juxtaposition of 60 successive snapshots like the ones shown on the right. They are separated by 4 ms. The snapshots have been shrunk along the horizontal axis in order to evidence the trajectory of the trimer and the plate. The plate motion is the sinusoidal curve at the bottom of each picture. The trimer motion can be seen as white sinusoids. The solid and the dashed vertical lines represent the snapshot from the second column ($t = 0$ ms) and from the third column, respectively.

The period-2 and period-3 modes are clearly visible along the first line and the third line of figure 5. It is remarkable to observe that the trimer experiences a jump of more than 2 cm before the three beads hit the plate simultaneously, the trimer plane being parallel to the plate during the whole flight. The contact between the plate and the beads is a bit particular for both modes. This is particularly clear when listening to the noise produced by the shocks when the trimer hits the plate. Indeed, when the period-2 or period-3 modes are obtained, the noise decreases drastically. The trimer comes in contact very softly and it looks like a more delicate landing. This means that the trimer and the plate have approximately the same speed. This can be due to the inelastic collapse of the trimer on the plate [3, 5], even if we do not have direct proof of chattering. The contact also lasts more than 10 ms. According to the observations, the rebound looks completely inelastic from the point of view of the plate. The memory of the previous bounce is completely erased.

The modes called twist-2 and twist-3 are the ones characterized by a succession of two bead contacts followed by the third bead contact. In figure 5, the twist is observed through the variation of the white area according to the inclination of the trimer. In the twist-3 mode, the time delay between the double impact and the single one is twice that of the time delay between the single impact and the double one. This asymmetry is not observed with the twist-2 mode but this may be due to a lack of time resolution. The movie diag.mov, available from stacks.iop.org/NJP/11/033016/mmedia, shows the modes period-2, twist-2, period-3 and twist-3 and their positions in the phase diagram (Γ, Δt).

The high-speed camera recordings have shown that the contacts between the trimer and the plate are persistent in the period-2 and period-3 modes. Moreover, the intensity of the hits is decreased in these modes, the noise generated by the collision being lower in these modes. The persistence of the contact is the ingredient that explains why the modes are observed at a given reduced acceleration that does not depend on the frequency (see figure 2(a)). Actually, the mechanism is as follows: under certain conditions that we will determine below, the trimer lands on the plate with a relative speed very close to zero. According to the relation equation (2), the memory of the previous jump is erased and the contact persists until the acceleration of the plate becomes equal to $-g$. At this moment, the trimer takes off with a speed equal to that of the plate. The motion is periodic if, after experiencing a parabolic flight, the trimer lands on the plate with a relative speed very close to zero.

The phase at which the trimer takes off and the speed of the trimer at the take-off can be easily determined. Knowing these initial conditions, the conditions on the frequency and on the reduced acceleration of the plate are deduced (i) by equating the parabolic flight and the motion of the plate and (ii) by imposing to zero the relative speed of the trimer and the plate at landing.

The equations of motion of the plate are

$$z = A\sin(\omega t), \tag{7}$$

$$\dot{z} = A\omega\cos(\omega t), \tag{8}$$

$$\ddot{z} = -A\omega^2\sin(\omega t), \tag{9}$$

where z is the vertical coordinate. The take-off phase δ is deduced from

$$-A\omega^2\sin(\delta) = -g. \tag{10}$$

The take-off phase is then equal to $\delta = \arcsin(\Gamma^{-1})$. The trimer and the plate have at the take-off moment the same vertical position z_0 and the same speed v_0

$$x_0 = \frac{g}{\omega^2}, \tag{11}$$

$$v_0 = \frac{g}{\omega}\sqrt{\Gamma^2 - 1}. \tag{12}$$

It is convenient to choose $t = 0$ at the take-off phase. The equation of motion of the plate becomes

$$z = A\sin(\omega t + \delta), \tag{13}$$

$$\dot{z} = A\omega\cos(\omega t + \delta). \tag{14}$$

After the take-off, the trimer experiences a parabolic flight until it hits the plate again. We impose that the speeds of the trimer and of the plate are the same at the moment of this contact. These constraints are written as follows:

$$1 + \sqrt{\Gamma^2 - 1}\omega t - \tfrac{1}{2}(\omega t)^2 = \Gamma\sin(\omega t + \delta), \tag{15}$$

$$\sqrt{\Gamma^2 - 1} - \omega t = \Gamma\cos(\omega t + \delta). \tag{16}$$

Equation (15) expresses the collision between the trimer and the plate, and equation (16) imposes that the speed of the trimer is the same as the speed of the plate. By taking the squares of both equations and after addition, the solution for ωt is very simple

$$\omega t = 2\sqrt{\Gamma^2 - 1}. \tag{17}$$

Substituting equation (17) into equation (15), we obtain

$$\sin\left(2\sqrt{\Gamma^2 - 1} + \arcsin(\Gamma^{-1})\right) = \Gamma^{-1}, \tag{18}$$

which is only possible if $2\sqrt{\Gamma^2 - 1} = (2n + 1)\pi$, where n is an integer different from 0. In other words, the persistent contact modes that are periodic orbits occur only for specific reduced accelerations Γ_n given by

$$\Gamma_n = \sqrt{\frac{(2n+1)^2}{4}\pi^2 + 1}. \tag{19}$$

This formula is valid for the ball, the dimer and the trimer. Period-1 (not observed) occurs at $\Gamma_0 = 1.86$, while period-2 and period-3 should occur at $\Gamma_1 = 4.82$ and $\Gamma_2 = 7.92$, respectively. These values are indicated by arrows in figure 3 showing good agreement with the experimental data. First of all, this model explains why period-2 and period-3 modes do occur at a certain

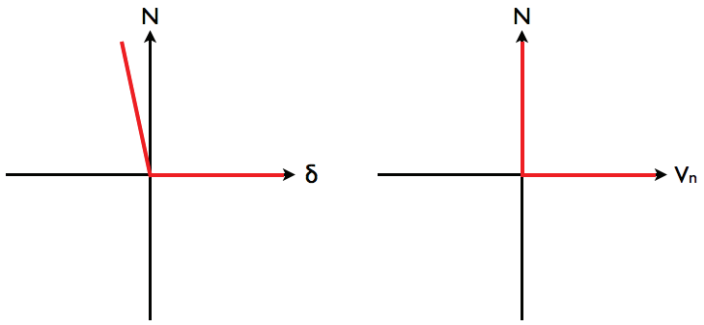

Figure 6. Illustration of Signorini's diagrams. The left diagram is smooth and presents the relation between normal force N and distance between the bodies δ. The right diagram is non-smooth and presents the relationship with normal relative velocity v_n instead of gap δ.

reduced acceleration. Neither the frequency nor the coefficient of restitution intervenes in the determination of the accelerations required for obtaining these periodical modes.

In the phase diagram figure 2(a), the period-2 and period-3 modes have not been observed above 75 Hz. This strongly suggests that the erasing of the previous jump is not total. The persistent time upper boundary can be taken as $1/(2f)$ (half of a period). Applying this to our present system, a contact may be qualified as persistent when it lasts longer than 7 ms. A contact that lasts less than this limit cannot suppress the impact history of the object.

4. Numerical simulation

4.1. Numerical method

The numerical simulations help in the determination of the phases at which a bead of the trimer hits the plate. In order to obtain the contact phase map, the main difficulty that the simulations have to tackle is the multiple contact management. In particular, the interaction between the resulting forces after the collision may generate frustration that is pretty hard to resolve numerically. The determination of the restitution coefficient illustrates this problem. When a single ball is concerned, it is very easy to define the restitution: the speed before and after the shock can be measured and the ratio determines the coefficient of restitution that eventually depends on the initial speed. On the other hand, the situation is more complicated when a multiple bead object is considered. For a dimer, ε depends on the angle that the dimer makes with the horizontal at the moment of the shock. The coefficient of restitution depends on the angle, the angular speed and the speed of the centre of mass. For the trimer, another degree of freedom has to be added. The energy dissipation due to the shock between a multiple bead object and the substrate finds its origin in the elastic dissipation when the trimer is bent and the friction between the beads and the substrate.

Similar to other models of the discrete element method (DEM), the non-smooth contact dynamics (NSCD) solves the contact forces in the local bases of the contacts [27]–[31]. The force is considered as the sum of the normal N and the tangential T components. In molecular dynamics models, the normal and tangential forces are usually estimated via the smooth Signorini and Coulomb diagrams illustrated in figures 6 and 7, respectively (plots on the left).

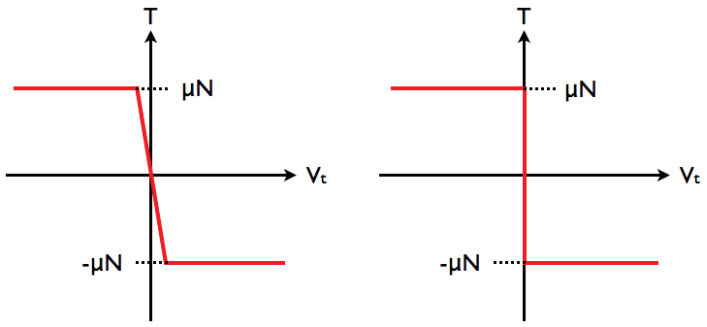

Figure 7. Illustration of Coulomb's diagrams. This diagram shows the relationship between the tangential force and the tangential relative velocity. The left diagram is smooth and the right one is a non-smooth representation.

The normal force is univocally determined as a function of the gap δ (distance between the bodies in contact).

The NSCD uses a non-smooth Signorini diagram (see figure 6, right) for the determination of the normal force at a contact. The particularity of this model is to consider this diagram not as a function of the distance between grains but as a function of the relative normal velocity v_n between the bodies in contact. The main consequence of this is the existence of a wide indetermination when the relative velocity is null. To avoid this indetermination, another relation between the normal force and the relative velocity must be defined (see below). The tangential force is estimated via the non-smooth Coulomb diagram (see figure 7, right) that is a consequence of the friction between the grains. In this case, the model deals again with the relative velocity between the grains in contact. The indetermination appears when the tangential relative velocity is null, i.e. when the body rolls without sliding or when it is static.

To avoid the indetermination on both normal and tangential components of the contact forces, another relationship between the components and the relative velocities must be established. These relations are based on Newton's equation applied to the bodies that are in contact. Indeed, the relative velocities of grains are determined by considering the impulses and momenta acting on the grains in contact through Newton's equations. The equation system links all the contact forces and the resolution of this system allows us to construct the global force network.

The trimer is simulated by obliging the spheres to remain at a constant distance from each other. In so doing, there is no need for an explicit description of the inertia. The simulation procedure is as follows. The frequency and the amplitude of the plate are first fixed. The trimer is released at a slight angle to the horizontal plane in order to break the symmetry. The simulation runs with a time step of 4 μs. After 5 s of simulation, the time delays between shocks of the bead with the plate are recorded. Moreover, it is possible to distinguish which bead hits the plate. Finally, the phase is also recorded in order to better understand the motion of the bouncing trimer.

4.2. Results of the simulations

An example of the numerical bouncing dimer is shown in the movie num.mov, available from stacks.iop.org/NJP/11/033016/mmedia, for the following set of parameters: $\alpha_r = 5.6$, $f = 25$ Hz, $\Gamma = 9.69$, $\varepsilon = 0$ and $\mu = 1$. The movie on the left is recorded from the front, while

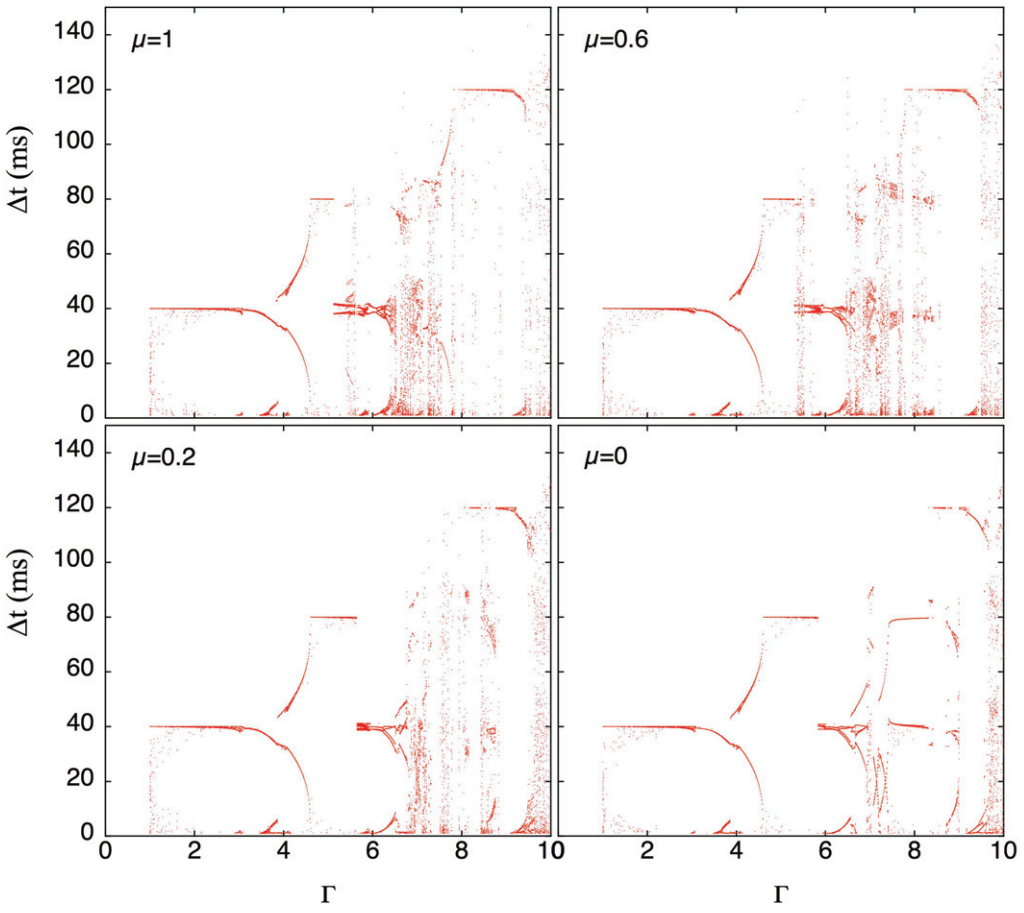

Figure 8. Comparison between numerical simulation results for four different friction coefficients: 0, 0.2, 0.6 and 1, while the coefficient of restitution of the bead is zero. The forcing frequency is 25 Hz.

the movie on the right is the view from the top in order to emphasize the horizontal excursion of the trimer.

The trimer with an aspect ratio of 5.6 has been tested for different values of the coefficient of restitution and of friction. To begin with, let us describe the result for $\varepsilon = 0$ and $\mu = 1$ represented in figure 8(a). The set of Δt between successive shocks of any bead of the trimer is plotted versus the reduced acceleration. The diagram is very similar to the experimental results (figure 3, bottom): (i) a plateau at 40 ms (25 Hz) for low acceleration; (ii) a bifurcation at $\Gamma = 4$; (iii) a period-2 plateau at $\Gamma = 5$; (iv) a large concentration of 40 ms events at $\Gamma = 6$; (v) a chaotic zone between $\Gamma = 7$ and 8; and (vi) finally a period-3 plateau at $\Gamma = 8$.

The modification of the coefficient of restitution has shown that this coefficient does not play a role. It does not drastically change the shape of the diagram $(\Gamma, \Delta t)$. On the other hand, the coefficient of friction does. In figure 8, the $(\Gamma, \Delta t)$ diagrams are represented for four friction coefficients: $\mu = 1$, 0.6, 0.2 and 0. The diagrams are the most complex when μ is high. Indeed, the dissipation is the highest and the rolling motion is predominant. The stability windows have slightly moved and are larger for low values of μ. Increasing the friction moves the stability windows towards lower reduced acceleration. The interpretation of this study

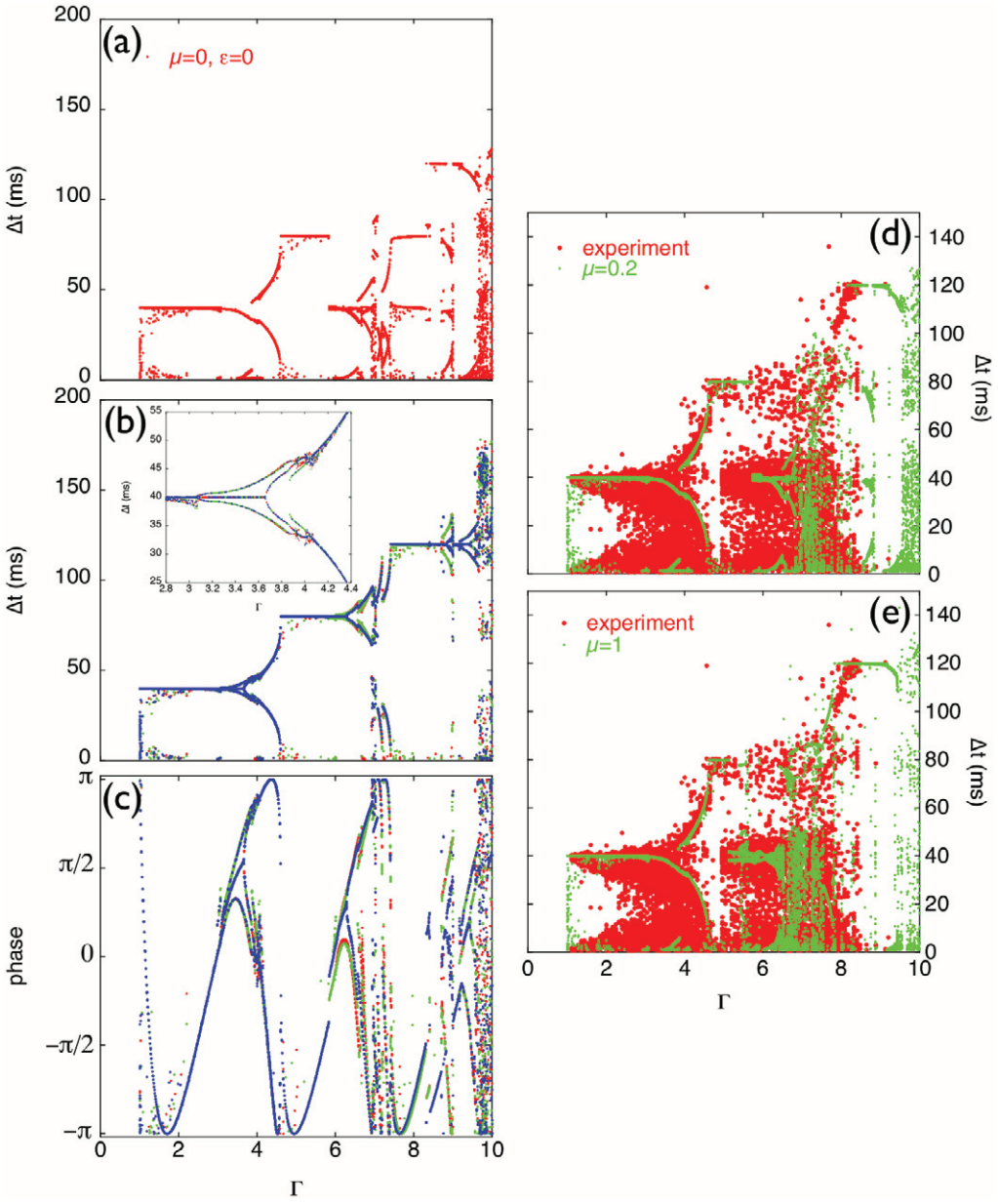

Figure 9. Comparison between the experimental and the simulation results. (a)–(c) Simulation of a bouncing trimer in which the aspect ratio is 5.6, the coefficient of restitution of one bead is zero and the coefficient of friction is zero. The forcing frequency is 25 Hz. (a) The classical (Γ, Δt) (figure 8, $\mu = 0$). With regard to this figure, the sets of time delay between two shocks for each particular bead are represented in (b). The different colours correspond to the different beads. (c) The phase of the plate at which each bead bounces. (d, e) Comparison of the numerical simulations ($\varepsilon = 0$, $\mu = 1$) and ($\varepsilon = 0$, $\mu = 0.2$) with the experimental results (all the points are shown).

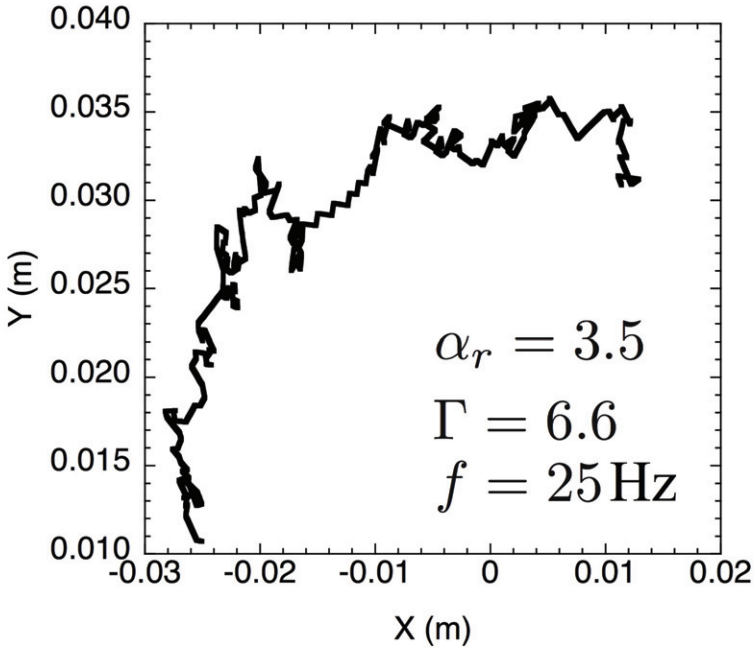

Figure 10. Trajectory of the centre of mass of a trimer in which the aspect ratio $\alpha_r = 3.5$. The trimer is shaken at a reduced acceleration $\Gamma = 6.6$ and the frequency is 25 Hz. The duration of the simulation is about 1 min.

reveals that the restitution and the dissipation laws of such a complex object have to be carefully determined. However, within this model, the general behaviour of the trimer has been very finely reproduced.

In figures 9(a)–(c), the bouncing of the trimer is analysed from: (a) the point of view of the sets of time delay between two successive contacts of any bead with the plate (as in the experimental process), (b) the time delays between two successive contacts with the plate for each individual bead (one colour per bead) and (c) the phases when a bead hits the plate (one colour per bead). The parameters used for the simulation are: a frequency of 25 Hz and a coefficient of restitution (of one bead) equal to 0. The comparison between the behaviour of the trimer and the individual beads allows us to show that degenerate modes exist. For example, around $\Gamma = 8$, all the beads hit the plate once every three periods but at different phases. As a result, the time delay between two successive shocks may exhibit only one branch (above $\Gamma = 8$) or three branches (below $\Gamma = 8$). The study of the individual bounces shows period doublings and bifurcations (emphasized by the insets). The beads do not play the same role and the initial conditions are of importance.

A direct comparison has been attempted using the experimental measurements for the restitution and the friction, $\varepsilon = 0.35$ and $\mu = 0.2$. In figures 9(d) and (e), the red points represent the time delay measurements for the trimer with respect to the acceleration Γ. It is from these measurements that the density plot (figure 3, bottom) has been deduced. Numerical simulations have been performed with the same restitution and friction and the collection of the time delays Δt is reported in figure 9(c). The behaviour of both sets of time delays are quite consistent. However, better agreement between experiment and theory is obtained when the chosen parameters are $\varepsilon = 0.35$ and $\mu = 1$. That means that the dissipative processes due to the flexion modes of the triangle between the beads should have been considered.

Finally, as shown in the movie num.mov, the numerical simulations are able to reproduce the random horizontal motion of the trimer. In figure 10, the trajectory of a 3.5 aspect ratio trimer is represented when it is shaken at $\Gamma = 6.6$ and at a frequency of 25 Hz. The motion time is about 1 min. The trajectory is very similar to that of figure 2(d). The characterization of the trajectory and the comparison with experimental data deserve additional investigations since the friction significantly influences the motion. Using numerical simulations, it will also be possible to determine the over- or under-diffusive behaviour of the trimer.

5. Conclusions

The complexity of an object placed on a shaker has been increased. Starting from a bouncing ball, to the dimer and ending with the trimer, the number of contacts between the object and the vibrating plate is increased. For the trimer, we found that several periodic modes can be observed such as rotation, period-2 and period-3 modes. The modes appear at a given reduced acceleration whatever the forcing frequency. High-speed camera recordings have allowed us to observe that the contact between the trimer and the plate is persistent between two successive jumps when the trimer bounces along the period-2 or period-3 modes. This is due to the fact that at the moment of the impact the relative speed between the trimer and the plate is zero. As a result, the memory of the jump previous to the contact is completely erased. The conditions for such behaviour have been modelled and we have shown that period-2 and period-3 are obtained for determined reduced accelerations Γ_n given by $\sqrt{(2n+1)^2\pi^2/4+1}$ for $n = 1$ and 2, respectively. It is remarkable that these conditions do not consider the coefficient of restitution, the friction and the shape of the particle. Our measurement has allowed us to give a criterion to define a persistent contact. In our system, a contact is persistent when it lasts longer than 7 ms because the period-2 and period-3 modes have not been observed above 75 Hz.

The rotation modes have been characterized. The period of rotation is proportional to the forcing frequency in the rotation-1 mode. This result is consistent with dimer measurements and theory [16]. These modes occur in stability windows of the bifurcation diagram that can be reproduced numerically. According to the numerical simulation, the main factor of dissipation has been found to be the coefficient of friction of the trimer with the plate.

Finally, self-propelled particle behaviour is found for the trimer when the condition of chaos is encountered. Numerical simulations have shown that the stability windows and bifurcation are very robust even when the coefficient of restitution and the friction are changed.

Acknowledgments

SD thanks the FNRS for financial support. T Gilet is acknowledged for fruitful discussions. Part of this work was supported by 'The Interuniversity Attraction Pole INANOMAT' (IAP P6/17).

References

[1] Lichtenberg M and Lieberman M 1983 *Regular and Stochastic Motion* (New York: Springer)
[2] Tufillaro N B, Abbot T and Reilly J 1992 *An Experimental Approach to Nonlinear Dynamics and Chaos* (New York: Addison-Wesley)
[3] Luck J M and Mehta A 1993 *Phys. Rev.* E **48** 3988
[4] Pieranski P 1983 *J. Physique* **44** 573

[5] Majundar S N and Kearney M J 2007 *Phys. Rev.* E **76** 031130
[6] Budd C J and Piiroinen P T 2006 *Physica* D **220** 127
[7] Luo G and Xie J 2001 *Physica* D **148** 183
[8] Koiller J, Markarian R, Kamphorst S O and de Carvalho S P 1995 *Nonlinearity* **8** 983
[9] Loskutov A, Ryabov A B and Akinshin L G 2000 *J. Phys. A: Math. Gen.* **33** 7973
[10] Pustyl'nikov L D 1995 *Russ. Math. Surv.* **50** 145
[11] Pastor J M, Maza D, Zuriguel I, Garcimartin A and Boudet J F 2007 *Physica* D **232** 128
[12] Umbanhowar P B and Swinney H L 1995 *Phys. Rev. Lett.* **75** 3838
[13] McNamara S and Falcon E 2005 *Phys. Rev.* E **71** 031302
[14] Poschel T, Brilliantov N V and Schwager T 2003 *Physica* A **325** 274
[15] Ben-Naim E and Krapivsky P L 2002 *Phys. Rev.* E **66** 011309
[16] Dorbolo S, Volfson D, Tsimring L and Kudrolli A 2005 *Phys. Rev. Lett.* **95** 044101
[17] Dorbolo S, Vandewalle N, Volfson D, Tsimring L and Kudrolli A 2005 *Powders and Grains 2005* ed R Garcia-Rojo, H J Herrmann and S McNamara (Rotterdam: AA Balkema)
[18] Wright H S, Swift M R and King P J 2006 *Phys. Rev.* E **74** 061309
[19] Bammert J, Schreiber S and Zimmermann W 2008 *Phys. Rev.* E **77** 042102
[20] von Gehlen S, Evstigneev M and Reimann P 2008 *Phys. Rev.* E **77** 031136
[21] Heinsalu E, Patriarca M and Marchesoni F 2008 *Phys. Rev.* E **77** 021129
[22] Kudrolli A, Lumay G, Volfson D and Tsimring L S 2008 *Phys. Rev. Lett.* **100** 058001
[23] Wright H S, Swift M R and King P J 2008 *Europhys. Lett.* **81** 14002
[24] Sharkovskii A N 1964 *Ukr. Math J.* **1** 61
[25] Li T Y and Yorke J A 1975 *Am. Math. Mon.* **82** 985
[26] Kaplan H 1987 *Am. J. Phys.* **55** 1023
[27] Jean M and Moreau J J 1992 *Proc. Contact Mech. Int. Symp.* pp 31–48
[28] Moreau J J 1994 *Eur. J. Mech.* A **13** 93–114
[29] Jean M 1995 *Frictional Contact in Rigid or Deformable Bodies: Numerical Simulation of Geomaterials* ed A P S Salvadurai and J M Boulon (Amsterdam: Elsevier) pp 463–86
[30] Jean M, Acary V and Monerie Y 2001 *Phil. Trans. R Soc.* A **359** 2497–518
[31] Ludewig F 2007 Contribution aux approches numériques de la densification d'assemblées granulaires *PhD Thesis* Université de Liège